


Photoproduction of doubly heavy baryons at future e^+e^- colliders

Xi-Jie Zhan^{⊗,*}, Xing-Gang Wu^{⊗,†} and Xu-Chang Zheng^{⊗,‡}

Department of Physics, Chongqing Key Laboratory for Strongly Coupled Physics, Chongqing University, Chongqing 401331, People's Republic of China

 (Received 6 May 2023; accepted 9 October 2023; published 31 October 2023)

The photoproduction of doubly heavy baryon ($\Xi_{cc}, \Xi_{bb}, \Xi_{bc}$) is investigated in the context of future high-energy and high-luminosity e^+e^- colliders. The study incorporates two sources of initial photons, namely the laser back-scattering photon and the Weizäcker-Williams approximation photon. Alongside the direct photoproduction via the subprocess $\gamma + \gamma \rightarrow \Xi_{QQ'} + \bar{Q} + \bar{Q}'$ ($Q^{(i)} = c, b$), the resolved photoproduction channels are specifically considered, encompassing the subprocesses $\gamma + g \rightarrow \Xi_{QQ'} + \bar{Q} + \bar{Q}'$, $g + g \rightarrow \Xi_{QQ'} + \bar{Q} + \bar{Q}'$, and $q + \bar{q} \rightarrow \Xi_{QQ'} + \bar{Q} + \bar{Q}'$ with $q = u, d, s$. Within the framework of nonrelativistic QCD, two $[cc(bb)]$ -diquark configurations, $\bar{3}[^3S_1]$ and $6[^1S_0]$, and four (bc) -diquark configurations, $(bc)\bar{3}[^3S_1]$, $(bc)_6[^1S_0]$, $(bc)_6[^3S_1]$, and $(bc)\bar{3}[^1S_0]$, are considered in the calculations. Numerical results show that the single resolved photoproduction processes provide dominant contributions under certain collision configuration. At the future e^+e^- colliders, the doubly heavy baryon generated via the photoproduction mechanism is promisingly observable and can be well-studied.

DOI: [10.1103/PhysRevD.108.074030](https://doi.org/10.1103/PhysRevD.108.074030)

I. INTRODUCTION

Baryon containing two heavy quarks, referred to as doubly heavy baryons, offer a simplified structure akin to heavy quarkonia, thus enabling rigorous theoretical analysis. The first suspected observation of Ξ_{cc}^+ was reported by the SELEX Collaboration [1,2] in 2002 and 2005. Lately, in 2017, the LHCb Collaboration identified another doubly heavy baryon, Ξ_{cc}^{++} , through the decay mode $\Xi_{cc}^{++} \rightarrow \Lambda_c^+ K^- \pi^+ \pi^+$, with $\Lambda_c^+ \rightarrow p K^- \pi^+$ [3]. Further validation came from the LHCb Collaboration, confirming this baryon's existence via the decay channel $\Xi_{cc}^{++} \rightarrow \pi^+ \Xi_c^+$ [4,5]. These observations render the doubly heavy baryon a valuable environment for investigating QCD. Due to its nonrelativistic nature and the strong-interaction confinement, the production of doubly heavy baryons involves nonperturbative effects that cannot be calculated using perturbative QCD. In the work by Ma *et al.* [6], the nonrelativistic QCD (NRQCD) [7] factorization framework was employed to describe the production process. This framework divides the process into two stages: the perturbative creation of a heavy-quark pair in a certain quantum

state, referred to as a diquark, followed by its nonperturbative transition into a baryon. By expanding in the small velocity (v_Q) of the heavy quark in the baryon's rest frame, two leading-order states of (cc) -diquarks were identified: $\bar{3}[^3S_1]$ and $6[^1S_0]$, each associated with a corresponding long-distance matrix element (LDME), namely $h_{\bar{3}}$ and h_6 . $\bar{3}[^3S_1](6[^1S_0])$ represents (cc) -diquark is in S -wave $^3S_1(^1S_0)$ and in the $\bar{\mathbf{3}}(\mathbf{6})$ color state, while $h_{\bar{3}}(h_6)$ depicts its nonperturbative transition probability into the baryon. Extensive theoretical investigations have delved into the production of doubly heavy baryons [8–36]. These investigations encompass direct production in pp , ep , $\gamma\gamma$, and e^+e^- collisions, as well as indirect production via the decays of Higgs bosons, W bosons, Z bosons, and top quarks. A dedicated generator, GENXICC [37–39], has been developed to simulate hadroproduction in pp collisions.

The e^+e^- collider offers two primary avenues for the direct production of the doubly heavy baryon $\Xi_{QQ'}$: production through e^+e^- annihilation and via the photoproduction mechanism. In this work, $\Xi_{QQ'}$ represents the baryon $\Xi_{QQ'q}$, where $Q(Q')$ stands for either a charm (c) or bottom (b) quark, and q corresponds to an up (u), down (d), or strange (s) quark. As for the photoproduction, $\Xi_{QQ'}$ can be produced via direct photon-photon fusion such as $\gamma + \gamma \rightarrow \Xi_{QQ'} + \bar{Q} + \bar{Q}'$. The collision photon may originate from either the bremsstrahlung of the initial e^+e^- particles or from the process of laser backscattering with e^+e^- . In addition to direct photoproduction, there are also processes called resolved photoproduction [40], where the photon undergoes resolution, and its parton participates in

*zhanxj@cqu.edu.cn

†wuxg@cqu.edu.cn

‡zhengxc@cqu.edu.cn

Published by the American Physical Society under the terms of the Creative Commons Attribution 4.0 International license. Further distribution of this work must maintain attribution to the author(s) and the published article's title, journal citation, and DOI. Funded by SCOAP³.

the ensuing hard processes. These resolved photoproduction channels share the same order of perturbative expansion as the direct approach, necessitating their inclusion in calculations. Noteworthy earlier studies [40–45] have indicated that these resolved channels tend to dominate the photoproduction of heavy quarkonium at e^+e^- colliders. Several next-generation e^+e^- colliders have been proposed, including the FCC-ee [46], the CEPC [47,48], and the ILC [49,50]. Designed to operate at varying high collision energies, along with unprecedented luminosities, these potent e^+e^- colliders hold the potential to serve as exceptional platforms for diverse research subjects.

This study is anchored in the NRQCD framework, where we investigate the photoproduction of $\Xi_{QQ'}$ at future e^+e^- colliders. In addition to the direct photoproduction channel $\gamma + \gamma \rightarrow \Xi_{QQ'} + \bar{Q} + \bar{Q}'$, we also incorporate the resolved photoproduction processes, encompassing $\gamma + g \rightarrow \Xi_{QQ'} + \bar{Q} + \bar{Q}'$, $g + g \rightarrow \Xi_{QQ'} + \bar{Q} + \bar{Q}'$, and $q + \bar{q} \rightarrow \Xi_{QQ'} + \bar{Q} + \bar{Q}'$, where $q = u, d, s$. Section II elucidates the calculation's formulation, while Sec. III presents numerical outcomes and ensuing discussions. Section IV provides a succinct summary.

II. FORMULATION

Based on the NRQCD factorization framework, the photoproduction cross section of $\Xi_{QQ'}$ at the e^+e^- collider can be expressed as

$$\begin{aligned} d\sigma\left(e^+e^- \rightarrow e^+e^-\Xi_{QQ'} + \bar{Q} + \bar{Q}'\right) &= \int dx_1 f_{\gamma/e}(x_1) \int dx_2 f_{\gamma/e}(x_2) \\ &\times \sum_{i,j} \int dx_i f_{i/\gamma}(x_i) \int dx_j f_{j/\gamma}(x_j) \\ &\times \sum_n d\hat{\sigma}(ij \rightarrow (QQ')[n] + \bar{Q} + \bar{Q}') \langle \mathcal{O}^{\Xi_{QQ'}}[n] \rangle. \end{aligned} \quad (1)$$

Here $f_{\gamma/e}(x)$ is the energy spectrum of the photon. $f_{i/\gamma}(i = \gamma, g, u, d, s)$ represents the Glück-Reya-Schienbein distribution function of parton i in photons [51]. $f_{\gamma/\gamma}(x) = \delta(1-x)$ is for the direct photoproduction process. $d\hat{\sigma}(ij \rightarrow (QQ')[n] + \bar{Q} + \bar{Q}')$ is the differential partonic cross section, which is calculated perturbatively. For baryon Ξ_{cc} and Ξ_{bb} , $n = \bar{3}[^3S_1]$ and $\bar{6}[^1S_0]$. For Ξ_{bc} , $n = \bar{3}[^3S_1]$, $\bar{6}[^1S_0]$, $\bar{3}[^1S_0]$, and $\bar{3}[^1S_0]$. $\langle \mathcal{O}^{\Xi_{QQ'}}[n] \rangle = h_n$ is the long distance matrix element (LDME). People usually employ potential model, mimicking the heavy quarkonium case, introduce and relate a wave function to $h_{\bar{3}}$ [8,52–55],

$$h_{\bar{3}} \simeq |\Psi_{QQ'}(0)|^2. \quad (2)$$

As for $h_{\bar{6}}$, there is no such relation and it is set to equal to $h_{\bar{3}}$ for simplicity. This assumption is grounded in NRQCD's power counting with respect to v_c , where both $h_{\bar{6}}$ and $h_{\bar{3}}$ hold

equivalent orders [6]. According to NRQCD, the bound state Ξ_{QQ} can be expanded into a series of Fock states,

$$\begin{aligned} |\Xi_{QQ}\rangle &= c_1(v)|(QQ)q\rangle + c_2(v)|(QQ)qg\rangle \\ &+ c_3(v)|(QQ)qgg\rangle + \dots \end{aligned} \quad (3)$$

Since a light quark can readily emit gluons, the constituents in Eq. (3) hold equivalent importance, specifically, $c_1 \sim c_2 \sim c_3$. Consider a QQ pair in the $\bar{3}[^3S_1]$ state; one of the heavy quarks can emit a gluon without altering the spin of the heavy quark. Subsequently, this gluon undergoes a splitting into a pair of light quarks $q\bar{q}$, permitting the heavy QQ pair to engage with the light q to compose Ξ_{QQ} . Similarly, for a QQ pair in the $\bar{6}[^1S_0]$ state, one of the heavy quarks can emit a gluon that retains the spin of the heavy quark unchanged. This emitted gluon then segregates into a light $q\bar{q}$ pair, and the light quarks also exhibit a propensity for gluon emission. Consequently, this heavy QQ pair can capture a light quark and a gluon to assemble into Ξ_{QQ} . This elucidates why $h_{\bar{6}}$ and $h_{\bar{3}}$ hold the same order in v_c . For simplicity, we assume $h_{\bar{6}} = h_{\bar{3}}$ in the ensuing computations. Notably, the LDMEs serve as overarching parameters beyond the perturbative components, implying that the outcomes can be readily refined upon acquisition of novel LDMEs.

As previously mentioned, the e^+e^- collider presents two primary sources of initial photons. The first emanates from the bremsstrahlung of the initial e^+e^- pairs, and its energy distribution can be well-delineated within the Weizäcker-Williams approximation (WWA) [56],

$$\begin{aligned} f_{\gamma/e}(x) &= \frac{\alpha}{2\pi} \left[\frac{1 + (1-x)^2}{x} \log \frac{Q_{\max}^2}{Q_{\min}^2} \right. \\ &\left. + 2m_e^2 x \left(\frac{1}{Q_{\max}^2} - \frac{1}{Q_{\min}^2} \right) \right], \end{aligned} \quad (4)$$

where $x = E_\gamma/E_e$ represents the fraction of longitudinal momentum carried by the photon, while α denotes the electromagnetic fine structure constant. $Q_{\min}^2 = m_e^2 x^2/(1-x)$ and $Q_{\max}^2 = (E\theta_c)^2(1-x) + Q_{\min}^2$, with $\theta_c = 32$ mrad defining the maximum scattered angular cut to ensure photon to be real. Here, $E = E_e = \sqrt{s}/2$ reflects the collision energy, defined as \sqrt{s} .

Another source is from the laser back-scattering (LBS) with e^+e^- and its spectrum function is [57]

$$f_{\gamma/e}(x) = \frac{1}{N} \left[1 - x + \frac{1}{1-x} - 4r(1-r) \right], \quad (5)$$

where $r = x/[x_m(1-x)]$, and the normalization factor,

$$\begin{aligned} N &= \left(1 - \frac{4}{x_m} - \frac{8}{x_m^2} \right) \log(1+x_m) \\ &+ \frac{1}{2} + \frac{8}{x_m} - \frac{1}{2(1+x_m)^2}. \end{aligned} \quad (6)$$

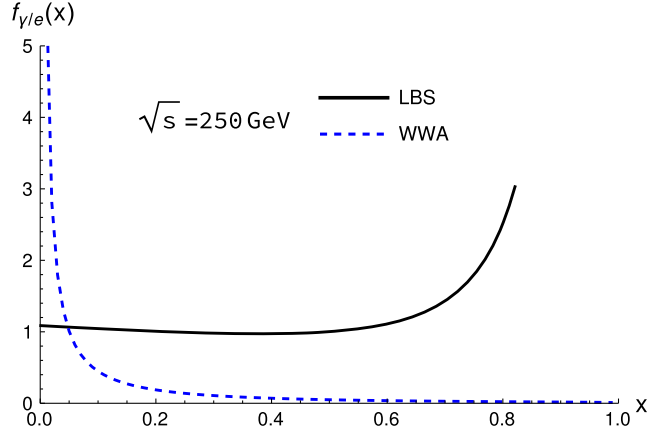


FIG. 1. The energy spectra of the LBS photon and the WWA photon.

Here $x_m = 4E_e E_l \cos^2 \frac{\theta}{2}$, E_e and E_l are the energies of incident electron and laser beams, respectively. θ is the angle between them. The energy of the LBS photon is restricted by

$$0 \leq x \leq \frac{x_m}{1 + x_m}, \quad (7)$$

with optimal value of x_m being 4.83 [58]. These two spectra have quite different behaviors as shown in Fig. 1.

Some typical Feynman diagrams for calculating the partonic cross sections are shown in Fig. 2. The well-established system Feynman diagram calculation [59] is used in the analytical and numerical calculations, where the standard projection method [60] is employed to deal with the amplitudes.

III. NUMERICAL RESULTS AND DISCUSSIONS

In the calculation, we take the wave functions at the origin as [54] $|\Psi_{cc}(0)|^2 = 0.039 \text{ GeV}^3$, $|\Psi_{bb}(0)|^2 = 0.152 \text{ GeV}^3$ and $|\Psi_{bc}(0)|^2 = 0.065 \text{ GeV}^3$. For consistency, we also

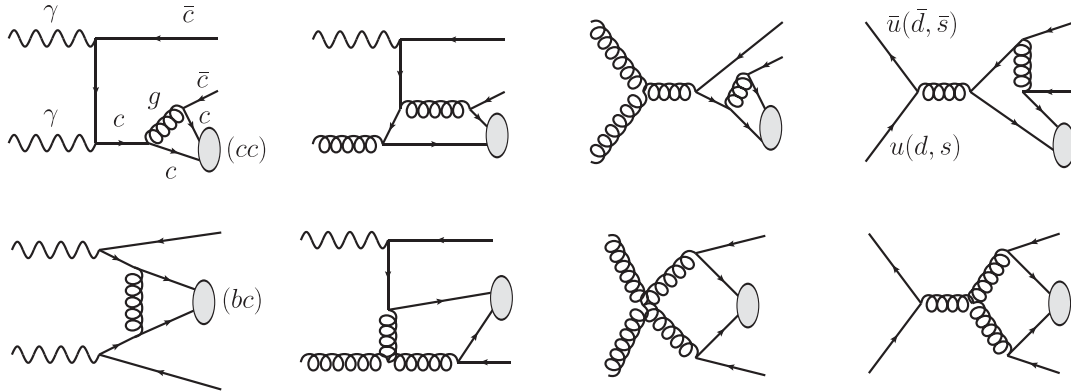


FIG. 2. Some typical Feynman diagrams for calculating the partonic cross section $\hat{\sigma}$ of $\Xi_{QQ'}$ photoproduction. The diagrams are drawn by JaxoDraw [61].

fix the quark masses as they are given in Ref. [54]; $m_c = M_{\Xi_{cc}}/2 = 1.8 \text{ GeV}$, and $m_b = M_{\Xi_{bb}}/2 = 5.1 \text{ GeV}$. The fine-structure constant is set to be $\alpha = 1/137$. As for the strong coupling constant, the one-loop running formulation is employed. The renormalization scale is by default taken as the transverse mass of $\Xi_{QQ'}$, $\mu = \sqrt{M_{\Xi_{QQ'}}^2 + p_t^2}$ with p_t representing its transverse momentum.

For collision energies of $\sqrt{S} = 250 \text{ GeV}$, 500 GeV , and 1000 GeV , along with the default inputs, Table I illustrates the cross section for the photoproduction of $\Xi_{QQ'}$ using both LBS and WWA photons (in brackets). This table includes a range of spin and color configurations. The results highlight a consistent trend; as collision energy increases, all cross sections exhibit growth, for the LBS photoproduction,

$$\begin{aligned} \sigma_{\Xi_{cc}}|_{250 \text{ GeV}} : \sigma_{\Xi_{cc}}|_{500 \text{ GeV}} : \sigma_{\Xi_{cc}}|_{1 \text{ TeV}} &\simeq 1 : 1.10 : 1.60, \\ \sigma_{\Xi_{bc}}|_{250 \text{ GeV}} : \sigma_{\Xi_{bc}}|_{500 \text{ GeV}} : \sigma_{\Xi_{bc}}|_{1 \text{ TeV}} &\simeq 1 : 1.15 : 1.69, \\ \sigma_{\Xi_{bb}}|_{250 \text{ GeV}} : \sigma_{\Xi_{bb}}|_{500 \text{ GeV}} : \sigma_{\Xi_{bb}}|_{1 \text{ TeV}} &\simeq 1 : 1.27 : 1.99, \end{aligned} \quad (8)$$

and for the WWA photoproduction,

$$\begin{aligned} \sigma_{\Xi_{cc}}|_{250 \text{ GeV}} : \sigma_{\Xi_{cc}}|_{500 \text{ GeV}} : \sigma_{\Xi_{cc}}|_{1 \text{ TeV}} &\simeq 1 : 1.79 : 2.93, \\ \sigma_{\Xi_{bc}}|_{250 \text{ GeV}} : \sigma_{\Xi_{bc}}|_{500 \text{ GeV}} : \sigma_{\Xi_{bc}}|_{1 \text{ TeV}} &\simeq 1 : 2.03 : 3.70, \\ \sigma_{\Xi_{bb}}|_{250 \text{ GeV}} : \sigma_{\Xi_{bb}}|_{500 \text{ GeV}} : \sigma_{\Xi_{bb}}|_{1 \text{ TeV}} &\simeq 1 : 2.50 : 5.05. \end{aligned} \quad (9)$$

The spin and color configurations also give different contributions to the total cross section and under $\sqrt{S} = 500 \text{ GeV}$ for the LBS photoproduction,

$$\begin{aligned} \sigma_{(cc)_3^3[S_1]} : \sigma_{(cc)_6^1[S_0]} &\simeq 10.63 : 1, \\ \sigma_{(bc)_3^3[S_1]} : \sigma_{(bc)_6^1[S_0]} : \sigma_{(bc)_6^3[S_1]} : \sigma_{(bc)_3^3[S_1]} &\simeq 4.71 : 1 : 2.36 : 2.00, \\ \sigma_{(bb)_3^3[S_1]} : \sigma_{(bb)_6^1[S_0]} &\simeq 11.14 : 1. \end{aligned} \quad (10)$$

TABLE I. The integrated cross sections (in units of fb) under default inputs for the photoproduction of $\Xi_{QQ'}$ via the LBS photon and the WWA photon (in brackets), respectively. Three typical collision energies are taken as example and intermediate diquark at various spin and color configurations are listed.

\sqrt{S} (GeV)	250	500	1000
$(cc)_3[{}^3S_1]$	733.68(62.75)	801.90(111.74)	1100.09(182.73)
$(cc)_6[{}^1S_0]$	65.65(2.79)	75.44(5.35)	105.89(9.35)
$(bc)_3[{}^3S_1]$	26.27(0.85)	30.44(1.73)	44.85(3.14)
$(bc)_6[{}^1S_0]$	5.72(0.18)	6.46(0.36)	9.44(0.66)
$(bc)_6[{}^3S_1]$	13.14(0.43)	15.22(0.86)	22.43(1.57)
$(bc)_3[{}^1S_0]$	11.45(0.35)	12.91(0.72)	18.88(1.32)
$(bb)_3[{}^3S_1]$	1.25(0.02)	1.56(0.05)	2.44(0.10)
$(bb)_6[{}^1S_0]$	0.09(0.0008)	0.14(0.002)	0.23(0.005)

The cross sections via the LBS photoproduction are much larger than those of the WWA. This is due to the quite different spectra functions of the photon as shown in Fig. 1. When assuming an integrated luminosity of $\mathcal{O}(10^4)$ fb $^{-1}$ at future e^+e^- colliders and aggregating contributions from all diquark configurations, approximately 8.8×10^6 (1.2×10^6) Ξ_{cc} , 6.5×10^5 (3.7×10^4) Ξ_{bc} , and 1.7×10^4 (4.9×10^2) Ξ_{bb} would be generated via LBS (WWA) photons, given a collision energy of $\sqrt{S} = 500$ GeV. The actual number of experimentally reconstructed events is significantly affected both by the decay rate of $\Xi_{QQ'}$ and the experimental reconstruction efficiency. Considering, for instance, the cascade decay $\Xi_{cc}^{++} \rightarrow \Lambda_c^+ K^- \pi^+ \pi^+ \simeq 10\%$ [62] and $\Lambda_c^+ \rightarrow p K^+ \pi^+ \simeq 5\%$ [63], and accounting for the experiment's reconstruction efficiency, the event count is expected to diminish by approximately three orders of magnitude. Consequently the photoproduction at future e^+e^- colliders could provides good opportunity to study Ξ_{cc} , while there would be not enough events for Ξ_{bb} .

Table II lists the contributions from different channels for the LBS photon. With the increase of collision energy, the cross sections of $\gamma + \gamma$ and $q + \bar{q}$ channels decrease, while those of the other two become larger. The $\gamma + g$ channels provide very important contributions at all these three collision energy and even dominant when the collision energy goes larger. The double-resolved channels, $g + g$ and $q + \bar{q}$, give very tiny productions which can be ignored compared with other two. Consequently for the LBS photon, the resolved photoproduction channel($\gamma + g$) at future e^+e^- colliders should be taken into account in the theoretical investigation. Conversely, in WWA photoproduction, the relative importance among various channels markedly deviates from that in LBS, as highlighted in Table III. The cross sections across all channels burgeon with increasing collision energy. While the direct $\gamma + \gamma$ channels consistently dominate, the contributions from other channels remain modest, and in certain cases, negligible.

Figure 3 illustrates the transverse momentum distributions of Ξ_{cc} and Ξ_{bc} photoproduction, with separate representations of contributions from different channels and intermediate diquark states. Each p_t distribution exhibits a discernible peak around several GeV, transitioning into a logarithmic decrease in the high p_t range. Throughout the entire p_t spectrum, the $3[{}^3S_1]$ configurations consistently hold prominence, rendering contributions from $6[{}^1S_0]$ states inconsequential. Specifically, in LBS photoproduction, the $\gamma + g$ channels dominate the lower p_t region, yielding the baton to the $\gamma + \gamma$ channels as the p_t value increases significantly. However, in practical experiments, there maybe not enough events in large p_t region to make precise measurements and consequently the single resolved channel $\gamma + g$ must be considered in the calculation of photoproduction. For the WWA case, the direct channel $\gamma + \gamma$ is always predominant in whole p_t region.

TABLE II. The integrated cross sections (in unit of fb) of different channels of the photoproduction of $\Xi_{QQ'}$ via the LBS photon. Three typical collision energies, 250(500, 1000) GeV, are taken and contributions of all intermediate diquark states have been summed up.

Channels	$\gamma + \gamma$	$\gamma + g$	$g + g$	$q + \bar{q}$
Ξ_{cc}	392.72(173.84, 70.13)	402.37(693.28, 1112.50)	3.22(9.35, 22.50)	1.02(0.88, 0.85)
Ξ_{bc}	32.85(16.02, 6.96)	23.00(47.31, 84.34)	0.36(1.37, 3.99)	0.37(0.33, 0.30)
Ξ_{bb}	0.80(0.44, 0.21)	0.51(1.20, 2.33)	0.0066(0.033, 0.11)	0.019(0.018, 0.017)

TABLE III. The integrated cross sections (in unit of fb) of different channels of the photoproduction of $\Xi_{QQ'}$ via the WWA photon. Three typical collision energies, 250(500, 1000) GeV, are taken and contributions of all intermediate diquark states have been summed up.

Channels	$\gamma + \gamma$	$\gamma + g$	$g + g$	$q + \bar{q}$
Ξ_{cc}	62.88(109.17, 172.06)	2.63(7.83, 19.77)	0.0088(0.042, 0.16)	0.023(0.047, 0.085)
Ξ_{bc}	1.71(3.32, 5.64)	0.09(0.34, 1.03)	0.00070(0.0045, 0.021)	0.003(0.008, 0.017)
Ξ_{bb}	0.02(0.04, 0.08)	0.0015(0.0068, 0.02)	$9.6 \times 10^{-6}(8.4 \times 10^{-5}, 4.8 \times 10^{-4})$	$9.7 \times 10^{-5}(2.8 \times 10^{-4}, 6.2 \times 10^{-4})$

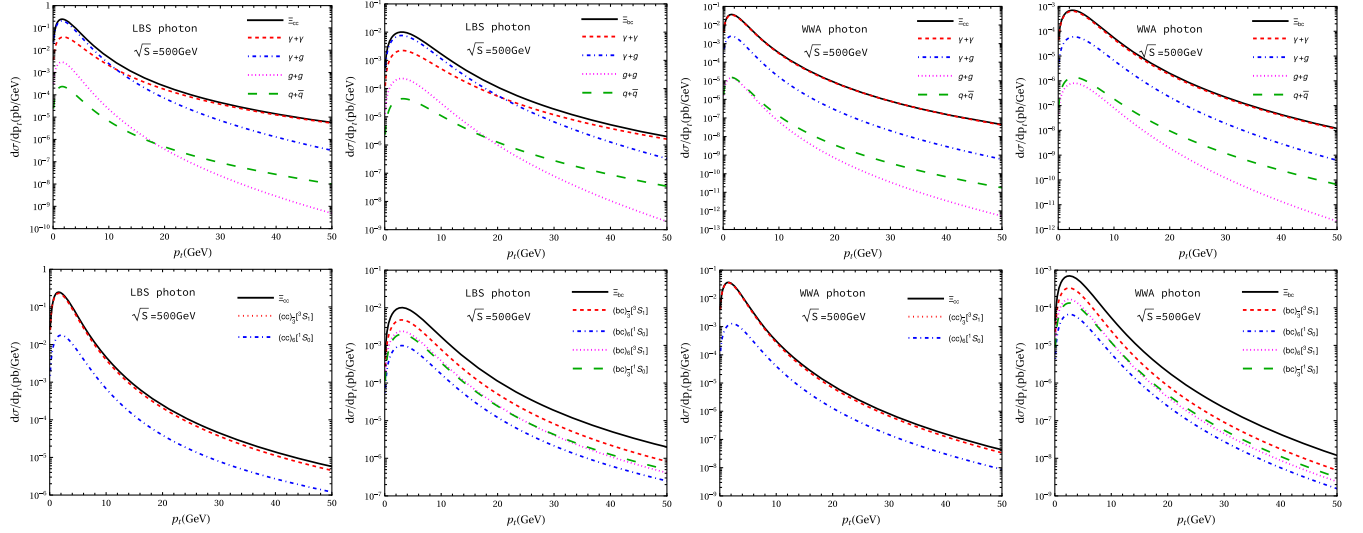


FIG. 3. The p_t distributions for Ξ_{cc} and Ξ_{bc} photoproduction under $\sqrt{S} = 500$ GeV and default values of the parameters. Figures in the first row are for different channels and those in the second row are for different intermediate diquark states. The topmost curve in every figure is their summation. Two columns of figures on the left are for LBS photon and those on the right are for WWA photon.

Figure 4 portrays the rapidity (y) distributions of Ξ_{cc} and Ξ_{bc} photoproduction. In the LBS scenario, the curves exhibit distinctive patterns across the central rapidity region, attributed to the prevalence of the $\gamma + g$ channel. In contrast to the transverse momentum (p_t) distribution, the $\gamma + g$ and $\gamma + \gamma$ channels do not intersect throughout the entire y range for a collision energy of $\sqrt{S} = 500$ GeV. Comparatively, the rapidity distributions of the WWA photoproduction appear conventional when juxtaposed with those of the LBS scenario.

Finally, we engage in a concise discussion on the theoretical uncertainties within our calculations, stemming from three primary sources: the heavy quark masses, the renormalization scale μ , and the LDMEs. Notably, uncertainties arising from h_3 and h_6 are omitted due to the

absence of reported errors in the literature. As previously indicated, these coefficients represent overall factors, and their impact on production outcomes can be readily refined with more accurate values. Table IV illustrates the effects of varying $m_c = 1.8 \pm 0.1$ GeV while holding $m_b = 5.1$ GeV and $\mu = \sqrt{M_{\Xi_{cc}}^2 + p_t^2}$ constant. Similarly, Table V presents uncertainties resulting from $m_b = 5.1 \pm 0.2$ GeV alongside $m_c = 1.8$ GeV and $\mu = \sqrt{M_{\Xi_{cc}}^2 + p_t^2}$. From these tables, even slight deviations in heavy quark mass can yield significant fluctuations in cross-section values. For instance, in Table IV, the cross section for $(cc)_3[{}^3S_1]$ varies by approximately 46% for a mere 12% alteration in m_c . This pronounced sensitivity is

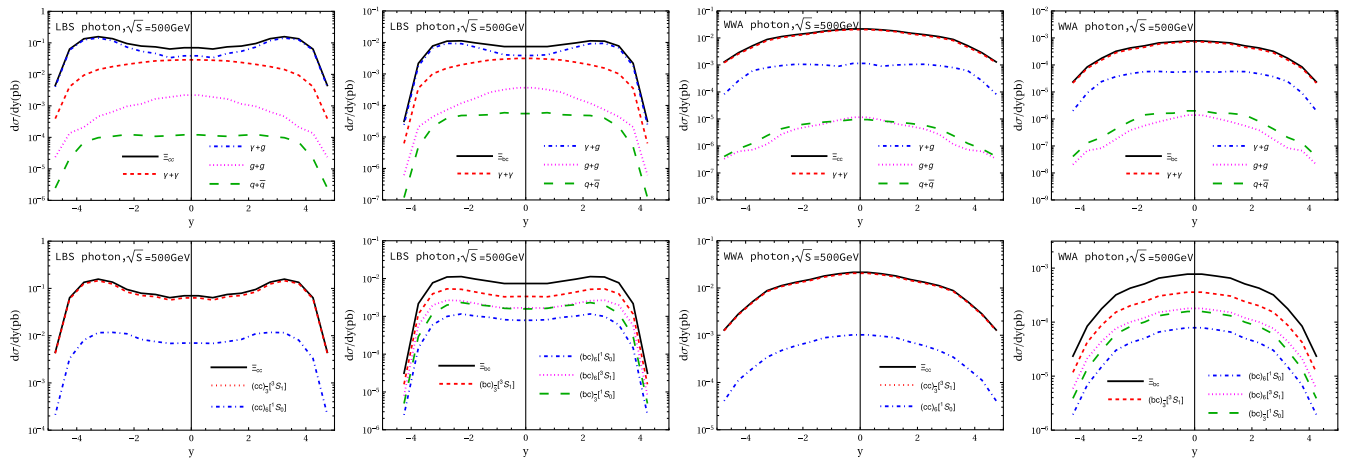


FIG. 4. The y distributions for Ξ_{cc} and Ξ_{bc} photoproduction under $\sqrt{S} = 500$ GeV and default values of the parameters. Figures in the first row are for different channels and those in the second row are for different intermediate diquark states. The topmost curve in every figure is their summation. Two columns of figures on the left are for LBS photon and those on the right are for WWA photon.

TABLE IV. The total cross sections (in units of fb) under different m_c for the $\Xi_{QQ'}$ production via the LBS photon and WWA photon (in brackets) at $\sqrt{S} = 500$ GeV, respectively. All subchannels have been summed up.

m_c (GeV)	1.7	1.8	1.9
$(cc)_{\bar{3}}[{}^3S_1]$	1104.64(159.47)	801.90(111.74)	594.56(79.88)
$(cc)_{\bar{6}}[{}^1S_0]$	104.07(7.66)	75.44(5.35)	55.80(3.81)
$(bc)_{\bar{3}}[{}^3S_1]$	36.10(2.05)	30.44(1.73)	25.86(1.47)
$(bc)_{\bar{6}}[{}^1S_0]$	7.74(0.43)	6.46(0.36)	5.45(0.31)
$(bc)_{\bar{6}}[{}^3S_1]$	18.05(1.03)	15.22(0.86)	12.93(0.73)
$(bc)_{\bar{3}}[{}^1S_0]$	15.47(0.85)	12.91(0.72)	10.89(0.62)

TABLE V. The total cross sections (in units of fb) under different m_b for the $\Xi_{QQ'}$ production via the LBS photon and WWA photon (in brackets) at $\sqrt{S} = 500$ GeV, respectively. All subchannels have been summed up.

m_b (GeV)	4.9	5.1	5.3
$(bc)_{\bar{3}}[{}^3S_1]$	35.25(2.05)	30.44(1.73)	26.39(1.47)
$(bc)_{\bar{6}}[{}^1S_0]$	7.42(0.43)	6.46(0.36)	5.62(0.31)
$(bc)_{\bar{6}}[{}^3S_1]$	17.63(1.02)	15.22(0.86)	13.19(0.73)
$(bc)_{\bar{3}}[{}^1S_0]$	14.84(0.86)	12.91(0.72)	11.23(0.61)

TABLE VI. The total cross sections (in units of fb) under various $\mu (= \mathcal{C}\sqrt{M_{\Xi_{QQ'}}^2 + p_t^2})$ with $\mathcal{C} = 0.5, 1, 2$ for the photoproduction of $\Xi_{QQ'}$ via the LBS photon and WWA photon (in brackets) at $\sqrt{S} = 500$ GeV, respectively. All subchannels have been summed up.

\mathcal{C}	0.5	1.0	2.0
$(cc)_{\bar{3}}[{}^3S_1]$	960.64(184.36)	801.90(111.74)	684.06(76.93)
$(cc)_{\bar{6}}[{}^1S_0]$	91.82(8.53)	75.44(5.35)	64.48(3.77)
$(bc)_{\bar{3}}[{}^3S_1]$	37.56(2.54)	30.44(1.73)	25.07(1.26)
$(bc)_{\bar{6}}[{}^1S_0]$	8.02(0.53)	6.46(0.36)	5.32(0.26)
$(bc)_{\bar{6}}[{}^3S_1]$	18.78(1.27)	15.22(0.86)	12.53(0.64)
$(bc)_{\bar{3}}[{}^1S_0]$	16.03(1.06)	12.91(0.72)	10.63(0.53)

illuminated when examining the pertinent Feynman diagrams, as exemplified in Fig. 2. For photoproduction of $\Xi_{QQ'}$ considered here, the final particles in the short-distance processes encompass solely Q and \bar{Q} ($Q = c$ or b), with corresponding internal lines comprising exclusively Q and gluon propagators. Hence, the profound influence of heavy quark masses on cross section appears reasonable. Let us take the second diagram ($\gamma + g \rightarrow c + c + \bar{c} + \bar{c}$) in the second row in Fig. 2 as an example, which is one of the predominant diagrams, to illustrate the strong dependence on m_c . The squared invariant mass of the gluon propagator that attached to the final $c\bar{c}$ pair is $k^2 = (p_c + p_{\bar{c}})^2$. Its dominant

region in phase space integration is near the threshold, i.e., $k^2 \sim 4m_c^2$. Consequently, when m_c changes from 1.7 GeV to 1.9 GeV, $1/(k^2)^2$ changes by about 36%. Table VI assesses the sensitivity to the renormalization scale ($\mu = \mathcal{C}\sqrt{M_{\Xi_{QQ'}}^2 + p_t^2}$, with $\mathcal{C} = 0.5, 1, 2$), considering fixed values for $m_c = 1.8$ GeV and $m_b = 5.1$ GeV. Evidently, substantial dependence on the renormalization scale is evident, potentially signifying the relevance of next-to-leading-order corrections in α_s . As we confront real-world measurements in the future, high-order calculations become imperative. Considering above uncertainties, the results in our leading-order calculation may fluctuate by about one order of magnitude. Within this range of variability, the photoproduction rates of doubly heavy baryons remain appreciable.

IV. SUMMARY

In this work, we have investigated the $\Xi_{QQ'}$ photoproduction within the framework of nonrelativistic QCD specifically focusing on future e^+e^- colliders. The investigation encompasses two distinct sources of initial photons; the LBS photon and the WWA photon. Two $[cc(bb)]$ -diquark configurations, $\bar{3}[{}^3S_1]$ and $\bar{6}[{}^1S_0]$, and four (bc) -diquark configurations, $(bc)_{\bar{3}}[{}^3S_1]$, $(bc)_{\bar{6}}[{}^1S_0]$, $(bc)_{\bar{6}}[{}^3S_1]$, and $(bc)_{\bar{3}}[{}^1S_0]$, are considered. Upon assuming $h_{\bar{6}} = h_{\bar{3}}$, the results demonstrate $\bar{3}[{}^3S_1]$ diquark state give dominant cross section, while other intermediate states also provide notable contributions. Importantly, beyond the direct photoproduction channel $\gamma + \gamma$, our study particularly integrates the resolved mechanisms, which are not fully considered in previous studies. Numeric findings underscore the critical role of the single resolved photoproduction channel $\gamma + g$ in LBS photoproduction, while its significance diminishes in the WWA scenario. If setting the integrated luminosity of future e^+e^- collision as $\mathcal{O}(10^4)$ fb $^{-1}$, there would be about 8.8×10^6 (1.2×10^6) Ξ_{cc} and 6.5×10^5 (3.7×10^4) Ξ_{bc} baryons to be generated via the LBS (WWA) photons respectively under the collision energy $\sqrt{S} = 500$ GeV. While acknowledging the relatively considerable uncertainties inherent in our calculations, we anticipate that these findings could serve as a valuable preliminary exploration into photoproduction at prospective e^+e^- colliders.

ACKNOWLEDGMENTS

This work was supported in part by the Natural Science Foundation of China under Grants No. 12147116, No. 12175025, No. 12005028, and No. 12147102, by the China Postdoctoral Science Foundation under Grant No. 2021M693743 and by the Graduate Research and Innovation Foundation of Chongqing, China under Grant No. ydstd1912.

- [1] M. Mattson *et al.* (SELEX Collaboration), *Phys. Rev. Lett.* **89**, 112001 (2002).
- [2] A. Ocherashvili *et al.* (SELEX Collaboration), *Phys. Lett. B* **628**, 18 (2005).
- [3] R. Aaij *et al.* (LHCb Collaboration), *Phys. Rev. Lett.* **119**, 112001 (2017).
- [4] R. Aaij *et al.* (LHCb Collaboration), *Phys. Rev. Lett.* **121**, 162002 (2018).
- [5] R. Aaij *et al.* (LHCb Collaboration), *Phys. Rev. Lett.* **121**, 052002 (2018).
- [6] J. P. Ma and Z. G. Si, *Phys. Lett. B* **568**, 135 (2003).
- [7] G. T. Bodwin, E. Braaten, and G. P. Lepage, *Phys. Rev. D* **51**, 1125 (1995); **55**, 5853(E) (1997).
- [8] S. P. Baranov, *Phys. Rev. D* **54**, 3228 (1996).
- [9] A. V. Berezhnoy, V. V. Kiselev, and A. K. Likhoded, *Z. Phys. A* **356**, 89 (1996).
- [10] J. Jiang, X.-G. Wu, Q.-L. Liao, X.-C. Zheng, and Z.-Y. Fang, *Phys. Rev. D* **86**, 054021 (2012).
- [11] J. Jiang, X.-G. Wu, S.-M. Wang, J.-W. Zhang, and Z.-Y. Fang, *Phys. Rev. D* **87**, 054027 (2013).
- [12] G. Chen, X.-G. Wu, Z. Sun, Y. Ma, and H.-B. Fu, *J. High Energy Phys.* **12** (2014) 018.
- [13] Z.-J. Yang, P.-F. Zhang, and Y.-J. Zheng, *Chin. Phys. Lett.* **31**, 051301 (2014).
- [14] Z.-J. Yang and X.-X. Zhao, *Chin. Phys. Lett.* **31**, 091301 (2014).
- [15] A. P. Martynenko and A. M. Trunin, *Phys. Rev. D* **89**, 014004 (2014).
- [16] X.-C. Zheng, C.-H. Chang, and Z. Pan, *Phys. Rev. D* **93**, 034019 (2016).
- [17] H.-Y. Bi, R.-Y. Zhang, X.-G. Wu, W.-G. Ma, X.-Z. Li, and S. Owusu, *Phys. Rev. D* **95**, 074020 (2017).
- [18] Z. Sun and X.-G. Wu, *J. High Energy Phys.* **07** (2020) 034.
- [19] G. Chen, X.-G. Wu, J.-W. Zhang, H.-Y. Han, and H.-B. Fu, *Phys. Rev. D* **89**, 074020 (2014).
- [20] G. Chen, X.-G. Wu, and S. Xu, *Phys. Rev. D* **100**, 054022 (2019).
- [21] G. Chen, C.-H. Chang, and X.-G. Wu, *Eur. Phys. J. C* **78**, 801 (2018).
- [22] A. P. Martynenko and A. M. Trunin, *Eur. Phys. J. C* **75**, 138 (2015).
- [23] S. Koshkarev, *Acta Phys. Pol. B* **48**, 163 (2017).
- [24] S. Koshkarev and V. Anikeev, *Phys. Lett. B* **765**, 171 (2017).
- [25] S. Groote and S. Koshkarev, *Eur. Phys. J. C* **77**, 509 (2017).
- [26] A. V. Berezhnoy, A. K. Likhoded, and A. V. Luchinsky, *Phys. Rev. D* **98**, 113004 (2018).
- [27] S. J. Brodsky, S. Groote, and S. Koshkarev, *Eur. Phys. J. C* **78**, 483 (2018).
- [28] A. V. Berezhnoy, I. N. Belov, and A. K. Likhoded, *Int. J. Mod. Phys. A* **34**, 1950038 (2019).
- [29] X.-G. Wu, *Sci. China Phys. Mech. Astron.* **63**, 221063 (2020).
- [30] Q. Qin, Y.-F. Shen, and F.-S. Yu, *Chin. Phys. C* **45**, 103106 (2021).
- [31] J.-J. Niu, L. Guo, H.-H. Ma, X.-G. Wu, and X.-C. Zheng, *Phys. Rev. D* **98**, 094021 (2018).
- [32] J.-J. Niu, L. Guo, H.-H. Ma, and X.-G. Wu, *Eur. Phys. J. C* **79**, 339 (2019).
- [33] P.-H. Zhang, L. Guo, X.-C. Zheng, and Q.-W. Ke, *Phys. Rev. D* **105**, 034016 (2022).
- [34] X. Luo, Y.-Z. Jiang, G.-Y. Zhang, and Z. Sun, *arXiv:2206.05965*.
- [35] X. Luo, H.-B. Fu, and H.-J. Tian, *Chin. Phys. C* **47**, 053102 (2023).
- [36] H.-H. Ma, J.-J. Niu, and X.-C. Zheng, *Phys. Rev. D* **107**, 014006 (2023).
- [37] C.-H. Chang, J.-X. Wang, and X.-G. Wu, *Comput. Phys. Commun.* **177**, 467 (2007).
- [38] C.-H. Chang, J.-X. Wang, and X.-G. Wu, *Comput. Phys. Commun.* **181**, 1144 (2010).
- [39] X.-Y. Wang and X.-G. Wu, *Comput. Phys. Commun.* **184**, 1070 (2013).
- [40] M. Klasen, B. A. Kniehl, L. N. Mihaila, and M. Steinhauser, *Phys. Rev. Lett.* **89**, 032001 (2002).
- [41] R. Li and K.-T. Chao, *Phys. Rev. D* **79**, 114020 (2009).
- [42] X.-J. Zhan and J.-X. Wang, *Eur. Phys. J. C* **80**, 740 (2020).
- [43] X.-J. Zhan and J.-X. Wang, *Chin. Phys. C* **45**, 023112 (2021).
- [44] X.-J. Zhan, X.-G. Wu, and X.-C. Zheng, *J. High Energy Phys.* **09** (2022) 050.
- [45] X.-J. Zhan, X.-G. Wu, and X.-C. Zheng, *Phys. Rev. D* **106**, 094036 (2022).
- [46] A. Abada *et al.* (FCC Collaboration), *Eur. Phys. J. Spec. Top.* **228**, 261 (2019).
- [47] C. S. Group, *arXiv:1809.00285*.
- [48] M. Dong *et al.* (CEPC Study Group), *arXiv:1811.10545*.
- [49] G. Aarons *et al.* (ILC Collaboration), *arXiv:0709.1893*.
- [50] J. Erler, S. Heinemeyer, W. Hollik, G. Weiglein, and P. M. Zerwas, *Phys. Lett. B* **486**, 125 (2000).
- [51] M. Gluck, E. Reya, and I. Schienbein, *Phys. Rev. D* **60**, 054019 (1999); **62**, 019902(E) (2000).
- [52] A. F. Falk, M. E. Luke, M. J. Savage, and M. B. Wise, *Phys. Rev. D* **49**, 555 (1994).
- [53] V. V. Kiselev, A. K. Likhoded, and M. V. Shevlyagin, *Phys. Lett. B* **332**, 411 (1994).
- [54] E. Bagan, H. G. Dosch, P. Gosdzinsky, S. Narison, and J. M. Richard, *Z. Phys. C* **64**, 57 (1994).
- [55] A. Berezhnoy, V. Kiselev, A. Likhoded, and A. Onishchenko, *Phys. Rev. D* **57**, 4385 (1998).
- [56] S. Frixione, M. L. Mangano, P. Nason, and G. Ridolfi, *Phys. Lett. B* **319**, 339 (1993).
- [57] I. F. Ginzburg, G. L. Kotkin, V. G. Serbo, and V. I. Telnov, *Nucl. Instrum. Methods Phys. Res.* **205**, 47 (1983).
- [58] V. I. Telnov, *Nucl. Instrum. Methods Phys. Res., Sect. A* **294**, 72 (1990).
- [59] J.-X. Wang, *Nucl. Instrum. Methods Phys. Res., Sect. A* **534**, 241 (2004).
- [60] G. T. Bodwin and A. Petrelli, *Phys. Rev. D* **66**, 094011 (2002); **87**, 039902(E) (2013).
- [61] D. Binosi and L. Theussl, *Comput. Phys. Commun.* **161**, 76 (2004).
- [62] F.-S. Yu, H.-Y. Jiang, R.-H. Li, C.-D. Lü, W. Wang, and Z.-X. Zhao, *Chin. Phys. C* **42**, 051001 (2018).
- [63] R. Aaij *et al.* (LHCb Collaboration), *J. High Energy Phys.* **12** (2013) 090.